

The Balloon-borne Large Aperture Submillimeter Telescope (BLAST)

Peter Ade^a, Itziar Aretxaga^b, James Bock^c, Jaspaul Chung^d, Mark Devlin^e, Simon Dicker^e, Edward Chapin^b, Matt Griffin^a, Joshua Gundersen^f, Mark Halpern^d, Peter Hargrave^a, David Hughes^b, Jeffrey Klein^e, Gaelen Marsden^d, Peter Martin^g, Phillip Maukopf^a, Barth Netterfield^g, Luca Olmi^h, Enzo Pascale^g, Marie Rex^e, Douglas Scott^d, Christopher Semisch^e, Matthew Truch^h, Carole Tucker^a, Greg Tuckerⁱ, Anthony Turner^c, Donald Weibe^g

^aUniversity of Wales, Department of Physics and Astronomy, 5, The Parade, P.O. Box 913, Cardiff, Wales, CF24 3YB, UK;

^bInstituto Nacional de Astrofísica, Óptica y Electrónica (INAOE), Apartado Postal 51 y 216, 72000, Puebla, Pue., MEXICO;

^cJet Propulsion Laboratory (JPL), 4800 Oak Grove Dr., M/S 169-327, Pasadena, CA 91109-8099, USA;

^dUniversity of British Columbia (UBC), Department of Physics and Astronomy, 6224 Agricultural Road., Vancouver, B.C. V6T 1Z1, CANADA;

^eUniversity of Pennsylvania, Department of Physics and Astronomy, 209 South 33rd St., Philadelphia, PA 19104, USA;

^fUniversity of Miami - Physics, James L. Knight Physics Building, 1320 Campo Sano Dr., Coral Gables, FL 33146, USA;

^gUniversity of Toronto, Department of Astronomy, 60 St. George St., Toronto, Ontario M5S 1A1, CANADA;

^hIstituto di Radio Astronomia, Largo E. Fermi 5, I-50125 Firenze, ITALY;

ⁱBrown University, Department of Physics, 182 Hope St., Providence, RI 02912, USA

ABSTRACT

Advances in bolometric detector technology over the past decade have allowed submillimeter wavelength measurements to contribute important data to some of the most challenging questions in observational cosmology. The availability of large format bolometer arrays will provide observations with unprecedented image fidelity. The Balloon-borne Large Aperture Submillimeter Telescope (*BLAST*) will be one of the first experiments to make full use of this new capability. The high altitude (≈ 35 km) of the balloon platform allows for high-sensitivity measurements in the 250, 350 and 500 μm bands with a total of 260 detectors.

Keywords: bolometers, detectors, arrays, galaxy evolution

1. INTRODUCTION

The Balloon-borne Large-Aperture Sub-millimeter Telescope (*BLAST*) flies from a Long Duration Balloon (LDB) platform. The telescope design incorporates a 2 m primary mirror with large-format bolometer arrays operating at 250, 350 and 500 μm . By providing the first sensitive large-area ($\sim 0.5 - 40$ deg²) submillimeter surveys at these wavelengths, *BLAST* will address some of the most important galactic and cosmological questions regarding the formation and evolution of stars, galaxies and clusters. Galactic and extragalactic *BLAST* surveys will: (i) identify large numbers of high-redshift galaxies; (ii) measure photometric redshifts, rest-frame FIR luminosities and star formation rates thereby constraining the evolutionary history of the galaxies that produce the FIR-submillimeter background; (iii) measure cold pre-stellar sources associated with the earliest stages of

Send correspondence to Mark Devlin. E-mail: devlin@physics.upenn.edu

star and planet formation; (iv) make high-resolution maps of diffuse galactic emission over a wide range of galactic latitudes. *BLAST* has been designed to fulfill these scientific goals as well as providing catalogues of > 3000 extragalactic submillimeter sources and a $\gg 100 \text{ deg}^2$ submillimeter galactic plane survey which will serve as a legacy to be followed at other wavelengths and resolutions, including sub-arcsecond imaging with ALMA.

The primary advantage of *BLAST* over existing submillimeter bolometer arrays such as SCUBA on the JCMT, and SHARC on the CSO (including their respective upgrades) is its greatly enhanced sensitivity at wavelengths $\leq 500 \mu\text{m}$ due to the dramatically increased atmospheric transmission at balloon altitudes. *BLAST* complements the *Herschel* satellite by testing identical detectors and filters planned for the SPIRE instrument.¹ Furthermore, the results from *BLAST* will be in time to influence the design (depth and area) of future SPIRE surveys. *BLAST* will complement the large-area spectroscopic galactic surveys of SWAS, provide submillimeter targets for the Fabry-Perot spectrograph SAFIRE on SOFIA, support the shorter wavelength mid-IR data of *SIRTF* and impact the design of the scientific case for the next generation of submillimeter surveys from space, e.g. SPECS, SPIRIT.

2. SCIENCE GOALS

BLAST will be the first long duration balloon-borne telescope to take advantage of the bolometric focal-plane arrays being developed for *Herschel*. The combination of northern and southern hemisphere LDB flights, providing the first surveys at 250, 350 and 500 μm , will significantly extend the wavelength range, sensitivity, and area of existing ground-based extragalactic and galactic surveys. Compared to the pioneering flights of PRONAOS,² *BLAST* will have an advantage of > 100 times the mapping speed. The scientific motivations for *BLAST* are similar to those of *Herschel* but are achievable with a series of LDB flights.

Using these unique *BLAST* surveys we expect to achieve the following science goals:

- Conduct a complementary series of wide (shallow) and narrow (confusion-limited) extragalactic 250–500 μm surveys, identifying the galaxy populations responsible for producing the far-IR and sub-mm backgrounds. *BLAST* will determine the amplitude of clustering of sub-mm galaxies on scales of 0.1–10 degrees, and ascertain whether this population of galaxies are the high- z progenitors of massive elliptical galaxies.
- Measure the 250–500 μm spectral energy distributions (SEDs) and colors to derive accurate photometric redshifts, and hence rest-frame luminosities and star formation rates (SFRs) for sub-mm selected galaxies.
- Measure the sub-mm source counts and place the strongest constraints to date on evolutionary models and the global star formation history of starburst galaxies at high- z .
- Conduct galactic surveys of the diffuse interstellar emission, molecular clouds, and identify dense, cold pre-stellar (Class 0) cores associated with the earliest stages of star formation.
- Observe Solar System objects including the Kuiper-belt objects, planets, and large asteroids.

3. EXTRAGALACTIC SURVEYS AT SUB-MILLIMETER WAVELENGTHS

Observations at sub-mm wavelengths of starburst galaxies in the high- z universe have two particular advantages compared to observations in the optical and FIR: a strong negative k -correction enhances the observed sub-mm fluxes, and sub-mm observations are significantly less affected by dust obscuration. SCUBA, and the millimeter camera MAMBO (operating on the IRAM 30 m), have now completed their first series of extragalactic sub-mm and mm (850 μm – 1.3 mm) surveys (^{3–11}). These ground-based surveys, which cover areas ranging from 0.002 to 0.2 deg^2 , are hundreds of times smaller than the proposed *BLAST* surveys (see Table 1). The SCUBA and MAMBO surveys have resolved 30–50% of the sub-mm/FIR background detected by COBE into individual sub-mm/mm galaxies, that appear to be associated with $z \gg 1$ Extremely Red Objects (EROs - IR galaxies which are extremely faint or undetected in the optical) and weak radio sources. The sub-mm source counts significantly exceed a no-evolution model and require strong evolution out to $z \sim 1$, but place weak constraints at higher redshifts since there is still vigorous debate on the overall redshift distribution. The source counts at bright sub-mm flux densities ($N_{850\mu\text{m}}(> 10\text{mJy})$) also show a large scatter (\sim a factor of 5) among different surveys that may be the result of clustering on the scale of these surveys, or indicative of a sharp cut-off in the luminosity function at $L_{\text{FIR}} > 10^{13} L_{\odot}$.

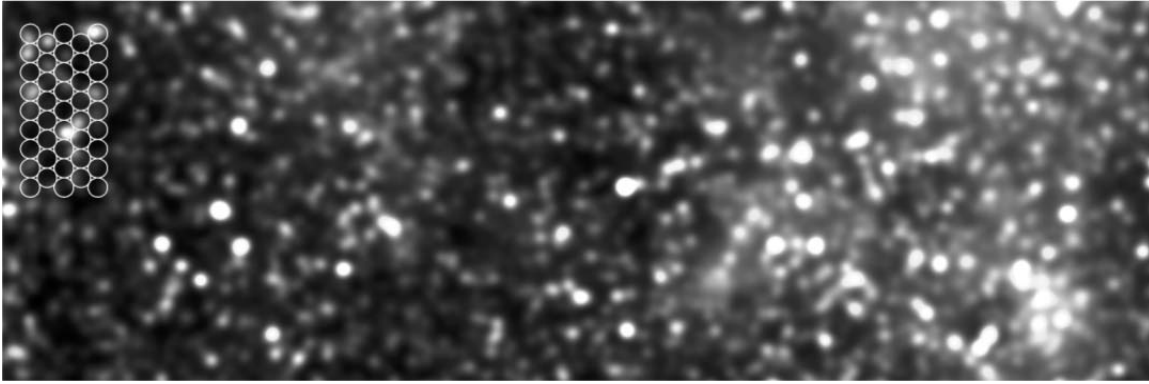


Figure 1. A simulated $0.5^\circ \times 1.0^\circ$, confusion-limited, *BLAST* survey made from the combination of data at 250, 350 and 500 μm . The assumptions for the evolution and clustering of submm galaxies are described in Hughes.¹² Extended cirrus emission is included in the simulations to test our source-extraction algorithms in the presence of this galactic foreground emission. The footprint of the 500 μm array is also shown.

3.1. *BLAST* Surveys

Wide-area *BLAST* surveys will be sensitive to star formation in the high- z universe and offer two important advantages over previous experiments. First, by providing accurate photometric redshifts from sub-mm colors for a significant number of sub-mm galaxies, *BLAST* will “break the redshift deadlock” (Hughes¹³ and Aretxaga¹⁴) that currently severely limits our understanding of the evolution of this galaxy population. Second, the sensitivity of the wide-area *BLAST* surveys are well-matched to the sensitivity of the current mm-interferometers. *BLAST* will provide $\gg 1000$ targets whose positions can be followed up with the SMA, CARMA and IRAM Plateau de Bure interferometers, providing positions with sub-arcsecond accuracy. These are necessary before deep IRAC imaging from *SIRTF* and NICMOS/HST observations can identify the faint IR counterparts. Even ALMA, with its powerful combination of sensitivity and resolution, will need extensive catalogues of sub-mm sources if the 64-element interferometer is to make the most efficient use of its longer baseline configurations.

Table 1. Estimated numbers and redshifts distribution of galaxies detected in nested LDB surveys.

50 hour 250 μm LDB survey strategies: $D=2.0$ m, $\text{NEFD}=236$ mJy $\text{s}^{1/2}$, $\theta = 30''$						
survey area (sq. degrees)	1σ depth	no. of pixels	no. of detected galaxies > 5σ	no. of detected galaxies > 10σ	no. of > 5σ galaxies $z > 1$	no. of > 5σ galaxies $z > 3$
1.0	5 mJy	18334	835	265	765	147
2.0	7 mJy	36668	1012	291	927	151
4.0	10 mJy	73336	1100	294	988	147
9.0	15 mJy	165006	1111	247	1023	129
36.0	30 mJy	660024	990	246	895	105

In addition *BLAST* will conduct nested surveys of various depths and areas (see Table 1) during Northern and Southern hemisphere LDB flights. Each LDB survey will be sensitive to a different population of sub-mm galaxies in the redshift/luminosity parameter space, and to clustering on different angular scales. The long-lasting legacy of each *BLAST* LDB flight will be an accurately calibrated catalogue of > 3000 sub-mm sources available for detailed spectroscopic and high-resolution observations with SOFIA, *SIRTF*, ALMA, GBT & LMT.

Hughes¹² has estimated that the extragalactic 3σ confusion limits of *BLAST* at 250–500 μm , assuming a primary mirror of 2 m, will be ~ 30 mJy (see Fig. 1). At these confusion limits, *BLAST* will detect $\sim 700 \pm 300$ sources/deg². *BLAST*, operating with a mirror which is 60% of the *Herschel* aperture and identical SPIRE

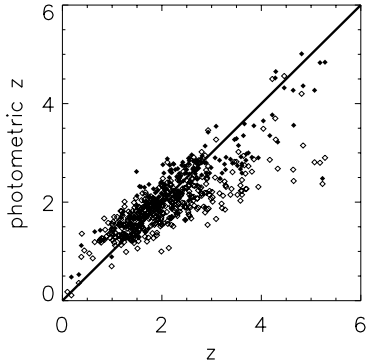


Figure 2. Photometric redshift vs. true redshift relationship for 424 mock galaxies simultaneously detected at 250, 350 and $500\mu\text{m}$ with *BLAST* in a simulated 1 deg^2 survey. The average photometric accuracy between $0 < z < 6$ is $\Delta z \sim \pm 0.6$. Further details of these simulations are given in Hughes.¹³ Open and filled symbols show the relationship inferred using only *BLAST* data, and the *BLAST* data plus SCUBA $850\mu\text{m}$ detections respectively, to derive the redshifts. The addition of $850\mu\text{m}$ measurements increases the accuracy of this method at $z \geq 4$.

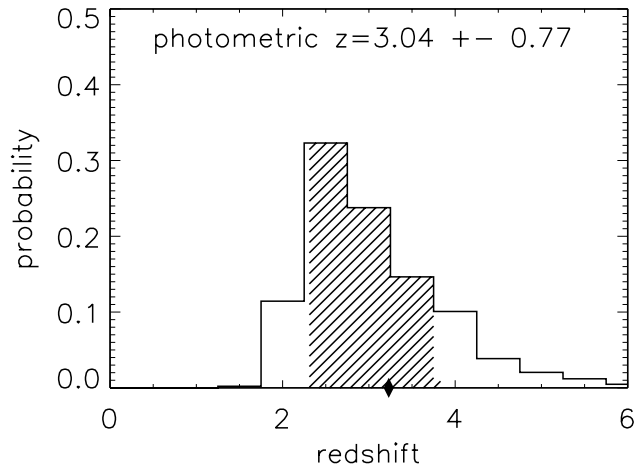


Figure 3. Redshift probability distribution derived from *BLAST* colors. The example shows the redshift distribution of a galaxy, detected in all three filters with a rest-frame FIR luminosity of $6 \times 10^{12} L_{\odot}$ at $z = 2.81$ (marked as a filled diamond). The galaxy has been selected from a mock catalogue of a survey with an absolute calibration error of 7% and measurement noise of 7 mJy. Other examples, and further explanation can be found in Hughes.¹³

filters, will provide the most accurate estimate of the extragalactic and galactic confusion levels for the SPIRE instrument. The instrumental performance and scientific results from a *BLAST* flight will therefore strongly influence the observing strategies for *Herschel*, including the decisions made on the depth and area of surveys.

3.2. The Evolutionary History of Galaxies Using Photometric Redshifts.

The primary science objective of *BLAST* is to determine the density of obscured star formation as a function of redshift. To achieve this goal, *BLAST* must first measure accurately the redshifts, temperatures, rest-frame FIR luminosities, SFRs, clustering properties and evolutionary histories of massive starburst galaxies. *BLAST* has therefore been designed to have extended wavelength coverage, low confusion limits, high atmospheric transparency and detector sensitivity, sufficient available observing time, and large areal coverage. Existing and planned telescopes (*e.g.* CSO, JCMT, IRAM, SOFIA, *SIRTF*, ISO) do not simultaneously address all of these issues.

Using Monte-Carlo simulations that take into account realistic absolute calibration errors ($\sim 7\%$), survey sensitivities, and the expected dispersion in the SEDs of high- z starburst galaxies (including any dependence of SED shape on bolometric luminosity), we have shown that it is possible to determine photometric redshifts from the *BLAST* colors, $S_{\text{mJy}}(250/350\mu\text{m})$ vs. $S_{\text{mJy}}(350/500\mu\text{m})$, with a precision of ± 0.6 (Hughes,¹³ see also Figs. 2 and 3). Given these redshifts, and constraints on the shape of the FIR-sub-mm SED, we can derive the rest-frame FIR luminosity (hence SFR) of an individual sub-mm galaxy. The precision improves as we extend the observational baseline to longer wavelengths. These extensive simulations show, however, that the *BLAST* data alone can measure the global star-formation history with an accuracy of $\pm 20\%$ for $z > 1$ (Fig. 4). This accuracy is due, in part, to the large sample size.

An important follow-up of the *BLAST* surveys will be mm-wavelength spectroscopic observations with the 100-m Green Bank Telescope (GBT), the 50-m Large Millimeter Telescope (LMT), the SMA and ALMA (> 2008). The detection of rotationally excited CO-lines in a sub-set of the *BLAST* sources will both determine the accuracy of the photometric-redshift technique, and provide estimates of mass, excitation, and dynamics of the molecular component in these high- z starburst galaxies. Even if redshifts can be obtained for a small number of optically-obscured sub-mm galaxies by other means, it will remain impossible to derive their rest-frame FIR luminosities

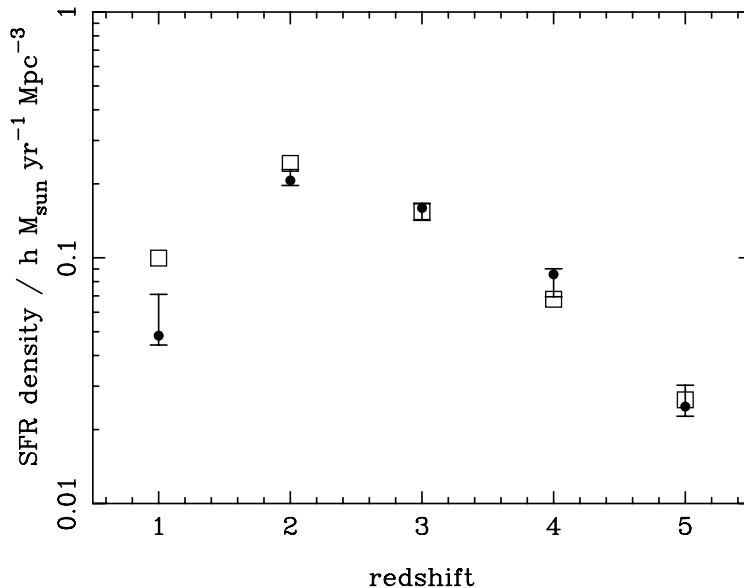


Figure 4. The global star formation history determined from simulated *BLAST* surveys. Star formation rates for individual galaxies are determined from the redshifts and FIR luminosities derived only from simulated *BLAST* observations at 250, 350 and 500 μm . The comparison of the input evolutionary model (open squares) with the global star formation level determined only from *BLAST* data (filled circles with 1σ errors) shows that *BLAST* can recover the global history of star formation to within a factor of 20% between $1.5 < z < 5.5$. This accuracy is due to the large statistical sample acquired from *BLAST* surveys. At $z \leq 1$ the *BLAST* bands do not sample the rest-frame FIR peak, limiting redshift determination in this range.

and SFRs for a statistically significant population without sensitive 250–500 μm observations of their SEDs from an experiment like *BLAST*.

3.3. The Statistics of *BLAST* Maps and Clustering of Galaxies.

A significant amount of additional information contained in the *BLAST* surveys will be found in one- and two-point statistics. While one-point statistics (usually referred to as $P(D)$ analysis, *i.e.* looking at histograms of pixel intensities), allow an estimate of source counts to be made well below the individual detection limit imposed by source confusion,^{4,15} two-point correlation statistics have been used to look at faint sources that produce fluctuations in the far-IR background (FIB)¹⁶ and in SCUBA maps.¹⁷ To date, only the Poisson fluctuations due to sources that are undetected individually have been measured. Correlations from clustering of the sub-mm sources has proved elusive. The amplitude of clustering of sub-mm bright galaxies, which are expected to be highly-biased, is entirely unknown at this point and strongly dependent on the redshift distribution of the sub-mm population. Estimates indicate that clustering of the galaxies which comprise the FIB can dominate over shot-noise on scales $> 10'$ (^{18–20}).

Our detailed simulations show that the *BLAST* surveys (0.5 – 40 deg²), which will combine a measure of the surface-density and spatial distribution of the brighter sub-mm sources (20 – 500 mJy) with photometric redshift information ($\Delta z \sim 0.6$), can provide the first robust determination of the clustering properties of sub-mm galaxies, the evolutionary model that describes their star-formation history,^{21–24} and hence discriminate between different scenarios of galaxy formation.

4. INSTRUMENT

The design and specifications of *BLAST* are driven by science goals, availability of existing instrumentation, and the practical limitations of ballooning. The decision to use an LDB platform for this experiment takes into consideration sensitivity, cost, and time-scale. The instrument will make use of, and test, state-of-the-art detectors and other systems that will be included on future ground and space-based missions. The scientific goals described here can be achieved from a LDB experiment, and the results used to help guide future satellite missions.



Figure 5. The *BLAST* mirror. The 2 m diameter carbon fiber mirror is made by Composite Optics Incorporated. It weighs 32 kg and has a surface rms of $2.4\mu\text{m}$.

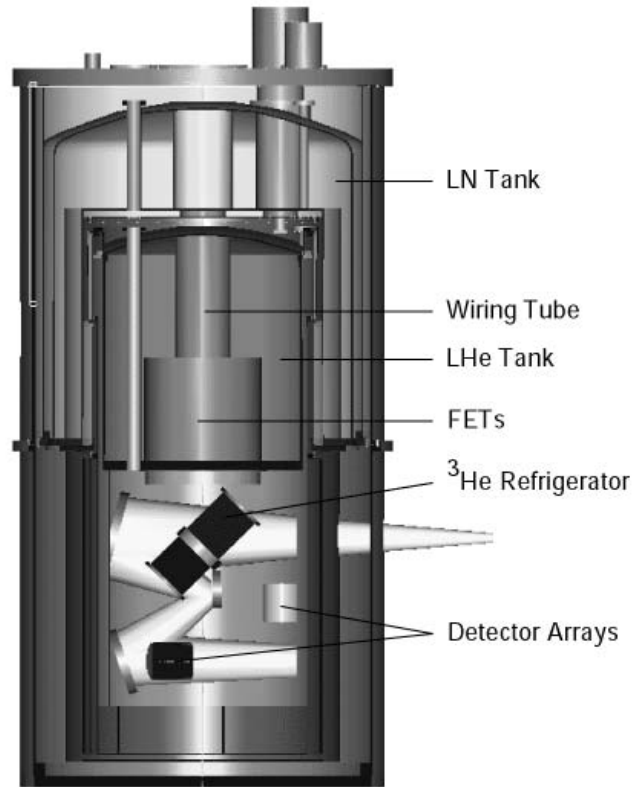


Figure 6. Cutaway view of the *BLAST* cryostat and cold re-imaging optics. The cryostat is 140 cm high.

4.1. Optical Design:

The *BLAST* gondola incorporates a 2 m carbon-fiber primary mirror. The spherical mirror has a mass of 32 kg and a surface rms of 2.4 microns. The mirror was designed and built by Composite Optics Incorporated*. A 50 cm diameter correcting secondary mirror gives diffraction limited performance over a $14' \times 7'$ FOV at the Cassegrain focus at $\lambda = 250\mu\text{m}$. The estimated antenna efficiency is $\geq 80\%$, and is determined by a combination of the rms surface roughness of the primary and the quality of the re-imaging optics. The primary and secondary mirrors are shown in Fig. 5. A more complete discussion of the optics can be found in Olmi.²⁵

Radiation from the telescope enters the cryostat through a 7.7 cm diameter vacuum window near the Cassegrain focus. The $f/5$ Cassegrain focus of the telescope is about 18 cm behind the back surface of the primary mirror. The cryostat window is made from 0.002 in thick polypropylene, which has $< 0.1\%$ loss. Blocking filters at the intermediate cold stages of 77 K and 30 K reduces the radiation loading on the LHe to $< 10\text{ mW}$. Table 2 summarizes the telescope parameters.

The radiation will be re-imaged onto the three detector arrays using a pair of cooled off-axis ellipsoidal mirrors arranged in a “Gaussian beam telescope” configuration (Fig. 6). This configuration makes corrections for aberrations in the main telescope and provides a flat focal plane with phase centers independent of wavelength for single-mode Gaussian beams. A cold aperture or Lyot stop, located between the two re-imaging mirrors at the position of an image of the primary mirror, provides additional side-lobe rejection. The second conic mirror has a focal length equal to its distance from this aperture to ensure that all of the detectors in the array have illumination centered on the Lyot stop. The off-axis angle of the final re-imaging mirror allows us to place dichroic beam splitters in front of the focal plane, making possible simultaneous measurements by all three arrays at different wavelengths.

*Composite Optics Incorporated, 9617 Distribution Avenue, San Diego, CA 92121, <http://www.coi-world.com>

Table 2. *BLAST* Telescope and receiver parameters.

Telescope:	Temperature	300K (230K for North American Flight)		
	Used diameter	1.9 m (secondary mirror is pupil stop)		
	Emissivity	0.04		
Detectors:	Bolometer optical NEP	$3.0 \times 10^{-17} \text{ W}/\sqrt{\text{Hz}}$		
	Bolometer quantum efficiency	0.8		
	Bolometer feed-horn efficiency	0.7		
	Throughput for each pixel	$A\Omega = \lambda^2$ ($2.0f\lambda$ feed-horns)		
Bands:	Central wavelengths	250	350	500 μm
	Number of pixels	149	88	43
	Beam FWHM	30	41	59 arc-seconds
	Field of view for each array	6.5×13 arc-minutes		
	Overall instrument transmission	30%		
	Filter widths ($\lambda/\Delta\lambda$)	3		
	Observing efficiency	90%		

Table 3. *BLAST* loading, BLIP noise, and sensitivities.

Band (μm)	250	350	500
Background power (pW)	50	36	26
Background NEP ($\times 10^{-17} \text{ W}/\sqrt{\text{Hz}}$)	20	14	10
NEFD ($\text{mJy s}^{0.5}$)	236	241	239
$\Delta S(1\sigma, 1 \text{ hr})(1 \text{ sq. deg.})$ (mJy)	38	36	36
$\Delta S(1\sigma, 6 \text{ hr})(1 \text{ sq. deg.})$ (mJy)	15.5	14.7	14.6

4.2. Detectors:

The *BLAST* focal plane will consist of arrays of 149, 88 and 43 detectors at 250, 350, and 500 μm respectively (Table 2). The detectors will be silicon-nitride micromesh (“spider-web”) bolometric detectors coupled with $2f\lambda$ feedhorn arrays. The detector and feedhorn technologies are well established and have been tested using the BOLOCAM instrument on the CSO. The entire detector and array configuration is based on the SPIRE instrument detectors.^{26,27} Figures 7, 8, 9, and 10 show examples of *BLAST* and SPIRE bolometer arrays (250 and 500 μm), a close-up of a single pixel, and the array support structure with feedhorns. The sensitivity of the detectors is limited by photon shot-noise from the telescope. We expect a total emissivity for the warm optics of $\simeq 8\%$, dominated by blockage from the secondary mirror and supports. We estimate the optical efficiency of the cold filters and optics to be $e_{\text{opt}} \geq 0.3$, based on measurements with similar bolometers coupled to horn arrays at millimeter wavelengths in the BOLOCAM test dewar. The estimated detector loading and NEFDs are shown in Table 3.

The $2f\lambda$ feedhorn separation maximizes the sensitivity per detector, but sparsely fills the field of view. Compared to Nyquist-sampled bare arrays, feedhorn-coupled arrays require additional pointings, but have more throughput to the sky per pixel. The net result is that, when conducting surveys in a scan-mapping mode, a Nyquist-sampled bare array has a larger instantaneous sensitivity, compared to a feedhorn-coupled array by a factor of ≈ 1.7 (see Bock²⁶ and Griffin²⁸). Nyquist-sampled arrays, however, require 16 times more detectors.

The detectors are read out with an AC-biased differential circuit. The data acquisition electronics demodulate the detector signals to provide noise stability to low frequencies ($< 30 \text{ mHz}$), which allows the sky to be observed in a slowly-scanned mode. Slow scanning is preferable over a mechanical chopper for mapping large regions of sky to the confusion limit.

The pre-amplifiers consist of Siliconix U401 differential JFETs with 5-7 $\text{nV}/\sqrt{\text{Hz}}$ noise at $\nu > 100 \text{ Hz}$. We have designed and tested a compact 24 channel JFET module. The JFET modules are integrated into the design

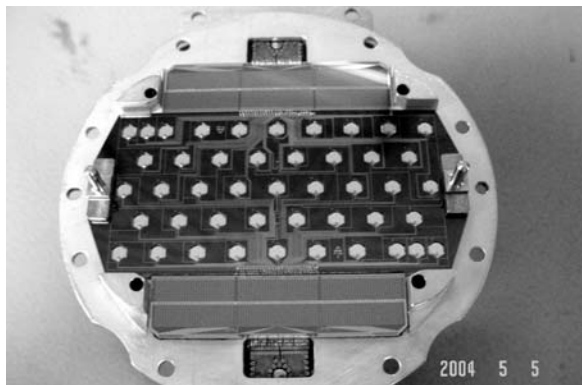


Figure 7. The 500 μm array of spiderweb bolometers mounted on the backshort array. The $\frac{1}{4}\lambda$ backshort is designed to maximize the power incident on the detector.

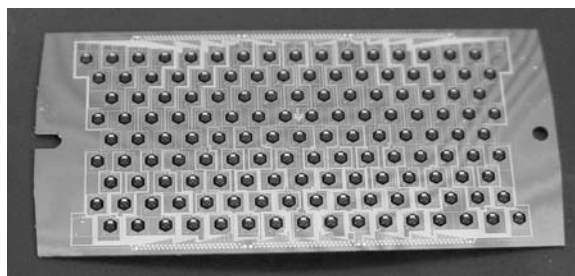


Figure 8. The 250 micron array. The physical size of the entire array is the same as the 500 micron array. The shorter wavelength allows more pixels to be fit into the focal plane.

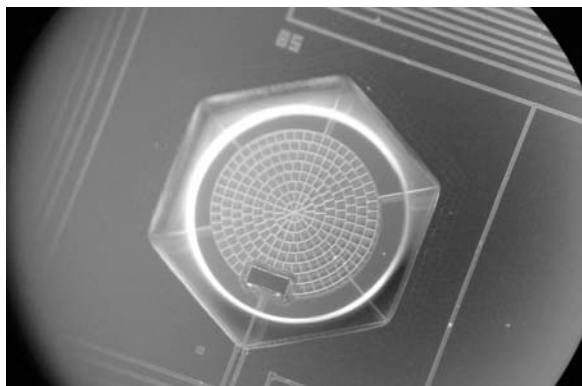


Figure 9. A single 500 micron pixel. This close-up view of the detector shows the details of the spiderweb structure and the thermistor.

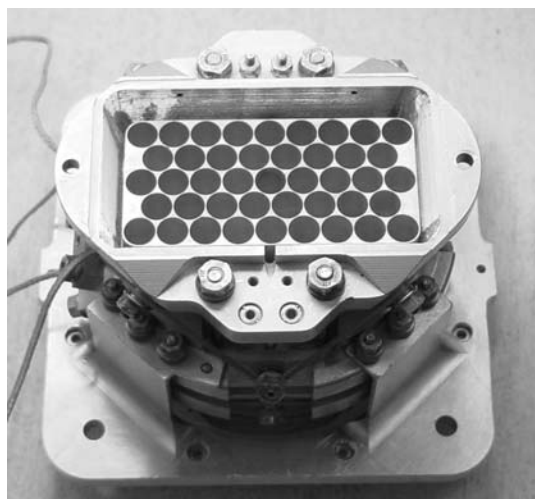


Figure 10. The bolometer and horn arrays (not shown) are mounted in the rectangular cavity in the bolometer detector module BDA. The 300 mK detectors and horns are suspended from the 2 K support structure with Kevlar fiber.

of the cryostat allowing us to sink their power dissipation (240 μW per pair) to the liquid nitrogen bath and decrease the load on the helium bath by approximately 60 mW.

The data is collected using a high-speed, flexible, 18-bit data acquisition system developed at the University of Toronto. The system can synchronously sample up to 600 channels at any rate up to 4 kHz. Each channel consists of a buffered input, a Sigma-Delta analog to digital converter with a digital anti-alias filter and an Altera programmable logic device (PLD). The firmware digitally demodulates each channel with the result stored to disk. This extremely flexible system is completed and was fully tested during the fall 2003 flight from Ft. Sumner, NM.

4.3. Cryogenics:

The receiver consists of an optical cavity inside a long hold-time liquid nitrogen and liquid helium cryostat (Fig. 6). Both the nitrogen and helium are maintained at slightly less than atmospheric pressure during the flight to minimize loss due to pressure drop at altitude.



Figure 11. The *BLAST* gondola prior to launch from Ft. Sumner, NM in September of 2003. The cable suspended gondola design is lightweight, has a high tensile strength, and a high resonant frequency.

A ^3He refrigerator maintains the detectors at 300 mK during flight. The self-contained, recycling refrigerator can maintain a base temperature of 280 mK with $30\ \mu\text{W}$ of cooling power for 4 days. It can be recycled within < 1 hr, and measures only 23 cm high by 12 cm in diameter. The ^3He refrigerator uses a pumped ^4He pot at $\approx 1\text{K}$ for cycling and to increase the hold time of the system. We currently have an operating system that will maintain a 1 K stage with 20 mW of cooling power with outside pressures ≤ 15 Torr. The entire optics box containing the re-imaging optics is also cooled to 1 K.

5. POINTING AND SCANNING

The pointing strategy is driven by three requirements: (i) in-flight pointing accuracy; (ii) in-flight positioning speed; and (iii) post-flight pointing reconstruction. Since *BLAST* is a mapping experiment, the in-flight pointing accuracy is not critical. Maximum in-flight absolute pointing errors of $2'$ are acceptable since they are small compared to the field of view. The stability of the bolometric detectors and the small atmospheric contribution at float eliminate the need for fast chopping. These facts coupled with a fast detector time constant (5 ms) enable the whole telescope to be positioned at a slew rate of $10'/\text{s}$. This positioning speed overcomes the $1/f$ noise in the detectors without smearing pixels. The most stringent pointing requirement is the post-flight reconstruction accuracy. Random reconstruction errors of $1/3$ of a beam-width would result in an acceptable $\approx 10\%$ degradation of the effective beam-size. However, source identification is more sensitive to systematic reconstruction errors, so our target accuracy is $1/5$ beam-width ($8''$).

The *BLAST* gondola consists of a precision-pointed inner frame (composed of the primary, secondary, near-field baffle, and cryostat) supported by an external gondola (see Fig. 11). The outer frame is pointed in azimuth by a flywheel and an active pivot. The inner frame has an elevation mount with direct-drive servo motors driving it relative to the outer frame. Balance of the inner frame is maintained by pumping liquid from one end of the frame to the other to compensate for cryogen blowoff.

5.1. Pointing Sensors:

The reconstruction of the absolute orientation of the telescope to 3" will be achieved using a 1317 x 1035 pixel, bore-sight mounted, CCD star camera capable of detecting 8.5 magnitude stars with 0.1 s of integration during the day at balloon altitudes. A 1.5 meter long, 30 cm diameter baffle extends beyond the camera to provide stray light rejection. The camera incorporates a f/2 lens with a 200 mm focal length. It has a $\approx 2 \times 2.5$ degree field of view. The full width half maximum of the image of a star is typically a few pixels, and centroiding techniques will be used to obtain sub-pixel resolution where a pixel corresponds to 7.8". There are typically as many as 20 stars of at least 8.5 magnitude in the camera's field at any given time. A real-time pattern recognition algorithm combines coarse attitude information from a 3-axis magnetometer (with $\pm 1.5^\circ$ azimuth, $\pm 0.5^\circ$ pitch and roll), the latitude and longitude information from a global positioning system, and the CCD image to make a rapid determination of the telescope's fine attitude. These data are used during the flight to update the gyros once/minute at the end points of a scan and after the flight to perform pointing reconstruction.

6. STATUS AND PLANS FOR BLAST

The *BLAST* instrument had its first engineering flight in the fall of 2003 from Ft. Sumner, NM. Only one array at 500 μm was available for the flight. This array was optimized for the background loading of the SPIRE instrument. The loading conditions on *BLAST* resulted in significantly reduced sensitivity. Since it was an engineering flight, we did not fly the carbon fiber mirror. Instead, we had a 1.9 meter aluminum mirror manufactured. In this configuration, we could test the system without risking losing our irreplaceable components.

The flight lasted 26 hours. We tested the detectors, cryogenics, electronics, pointing sensors and pointing systems. We obtained enough engineering data to complete the construction of the *BLAST* instrument. In particular the daytime star camera exhibited software and thermal problems during flight that have since been addressed.

We will fly the *BLAST* again in the fall of 2004 from Ft. Sumner, NM with 500 and 350 μm arrays which are optimized for balloon altitude loading conditions. We expect to make significant maps of galactic and some limited extragalactic regions.

In June of 2005 we will have an LDB flight from Kiruna, Sweden (Lat: 67°50'N, Lon: 20°25'E). This northern hemisphere flight will provide 5-7 days at float altitudes. We will have a full compliment of detectors and will fly the carbon fiber mirror. One advantage of flying a northern hemisphere flight first is that the recovery of the primary mirror is easier than from Antarctica. We will attempt an Antarctic flight in 2006.

ACKNOWLEDGMENTS

The *BLAST* collaboration acknowledges the support of NASA through grant number NAG5-12785, the Canadian Space agency, and the UK Particle Physics & Astronomy Research Council (PPARC) through the Cardiff Astronomy Instrumentation Group rolling grant. We would also like to thank the National Scientific Balloon Facility staff for their outstanding work.

REFERENCES

1. M. J. Griffin, B. M. Swinyard, and L. G. Vigroux, "SPIRE - Herschel's Submillimetre Camera and Spectrometer," in *IR Space Telescopes and Instruments. Edited by John C. Mather . Proceedings of the SPIE, Volume 4850, pp. 686-697 (2003).*, pp. 686-697, Mar. 2003.
2. J. M. Lamarre, M. Giard, E. Pointecouteau, J. P. Bernard, G. Serra, F. Pajot, F. X. Désert, I. Ristorcelli, J. P. Torre, S. Church, N. Coron, J. L. Puget, and J. J. Bock, "First Measurement of the Submillimeter Sunyaev-Zeldovich Effect," *ApJ* **507**, pp. L5-L8, Nov. 1998.
3. I. Smail, R. J. Ivison, and A. W. Blain, "A Deep Sub-millimeter Survey of Lensing Clusters: A New Window on Galaxy Formation and Evolution," *ApJ* **490**, pp. L5+, Nov. 1997.
4. D. H. Hughes, S. Serjeant, J. Dunlop, M. Rowan-Robinson, A. Blain, R. G. Mann, R. Ivison, J. Peacock, A. Efstathiou, W. Gear, S. Oliver, A. Lawrence, M. Longair, P. Goldschmidt, and T. Jenness, "High-redshift star formation in the Hubble Deep Field revealed by a submillimetre-wavelength survey.," *Nature* **394**, pp. 241-247, 1998.

5. A. W. Blain, I. Smail, R. J. Ivison, and J.-P. Kneib, “The history of star formation in dusty galaxies,” *MNRAS* **302**, pp. 632–648, Feb. 1999.
6. S. J. Lilly, S. A. Eales, W. K. P. Gear, F. Hammer, O. Le Fèvre, D. Crampton, J. R. Bond, and L. Dunne, “The Canada-United Kingdom Deep Submillimeter Survey. II. First Identifications, Redshifts, and Implications for Galaxy Evolution,” *ApJ* **518**, pp. 641–655, June 1999.
7. T. M. A. Webb, S. J. Lilly, D. L. Clements, S. Eales, M. Yun, M. Brodwin, L. Dunne, and W. K. Gear, “The Canada-UK Deep Submillimeter Survey. VII. Optical and Near-Infrared Identifications for the 14 Hour Field,” *ApJ* **597**, pp. 680–698, Nov. 2003.
8. C. L. Carilli, F. Owen, M. Yun, F. Bertoldi, A. Bertarini, K. M. Menten, E. Kreysa, and R. Zylka, “Wide Field Imaging at 250 GHz,” in *Deep Millimeter Surveys: Implications for Galaxy Formation and Evolution*, pp. 27–+, 2001.
9. S. E. Scott, M. J. Fox, J. S. Dunlop, S. Serjeant, J. A. Peacock, R. J. Ivison, S. Oliver, R. G. Mann, A. Lawrence, A. Efstathiou, M. Rowan-Robinson, D. H. Hughes, E. N. Archibald, A. Blain, and M. Longair, “The SCUBA 8-mJy survey - I. Submillimetre maps, sources and number counts,” *MNRAS* **331**, pp. 817–838, Apr. 2002.
10. S. C. Chapman, D. Scott, C. Borys, and G. G. Fahlman, “Submillimetre sources in rich cluster fields: source counts, redshift estimates and cooling flow limits,” *MNRAS* **330**, pp. 92–104, Feb. 2002.
11. T. M. Webb, S. A. Eales, S. J. Lilly, D. L. Clements, L. Dunne, W. K. Gear, R. J. Ivison, H. Flores, and M. Yun, “The Canada-UK Deep Submillimeter Survey. VI. The 3 Hour Field,” *ApJ* **587**, pp. 41–54, Apr. 2003.
12. D. H. Hughes and E. Gaztañaga, “Simulated Submillimetre Galaxy Surveys,” in *ESA SP-445: Star Formation from the Small to the Large Scale*, pp. 29–+, 2000.
13. D. H. Hughes, I. Aretxaga, E. L. Chapin, E. Gaztañaga, J. S. Dunlop, M. J. Devlin, M. Halpern, J. Gundersen, J. Klein, C. B. Netterfield, L. Olmi, D. Scott, and G. Tucker, “Breaking the ‘redshift deadlock’- I. Constraining the star formation history of galaxies with submillimetre photometric redshifts,” *MNRAS* **335**, pp. 871–882, Oct. 2002.
14. I. Aretxaga, D. H. Hughes, E. L. Chapin, E. Gaztañaga, J. S. Dunlop, and R. J. Ivison, “Breaking the ‘redshift deadlock’- II. The redshift distribution for the submillimetre population of galaxies,” *MNRAS* **342**, pp. 759–801, July 2003.
15. C. Borys, S. C. Chapman, and D. Scott, “Using SCUBA to place upper limits on arcsecond-scale cosmic microwave background anisotropies at $850\mu\text{m}$,” *MNRAS* **308**, pp. 527–538, Sept. 1999.
16. G. Lagache, J. Puget, A. Abergel, F. Desert, H. Dole, F. R. Bouchet, F. Boulanger, P. Ciliegi, D. L. Clements, C. Cesarsky, D. Elbaz, A. Franceschini, R. Gispert, B. Guiderdoni, L. M. Haffner, M. Harwit, R. Laureijs, D. Lemke, A. F. M. Moorwood, S. Oliver, W. T. Reach, R. J. Reynolds, M. Rowan-Robinson, M. Stickel, and S. L. Tufte, “The Extragalactic Background and Its Fluctuations in the Far-Infrared Wavelengths,” in *LNP Vol. 548: ISO Survey of a Dusty Universe*, pp. 81–+, 2000.
17. J. A. Peacock, M. Rowan-Robinson, A. W. Blain, J. S. Dunlop, A. Efstathiou, D. H. Hughes, T. Jenness, R. J. Ivison, A. Lawrence, M. S. Longair, R. G. Mann, S. J. Oliver, and S. Serjeant, “Starburst galaxies and structure in the submillimetre background towards the Hubble Deep Field,” *MNRAS* **318**, pp. 535–546, Oct. 2000.
18. Z. Haiman and L. Knox, “Correlations in the Far-Infrared Background,” *ApJ* **530**, pp. 124–132, Feb. 2000.
19. E. Gaztañaga and D. Hughes, “Clustering in Deep (Submillimeter) Surveys,” in *Deep Millimeter Surveys: Implications for Galaxy Formation and Evolution*, pp. 131–+, 2001.
20. L. Knox, A. Cooray, D. Eisenstein, and Z. Haiman, “Probing Early Structure Formation with Far-Infrared Background Correlations,” *ApJ* **550**, pp. 7–20, Mar. 2001.
21. B. Guiderdoni, E. Hivon, F. R. Bouchet, and B. Maffei, “Semi-analytic modelling of galaxy evolution in the IR/submm range,” *MNRAS* **295**, pp. 877–898, Apr. 1998.
22. A. Franceschini, P. Andreani, and L. Danese, “Millimetric properties of IRAS galaxies - III. Luminosity functions, sub-mm counts and contributions to the sky background,” *MNRAS* **296**, pp. 709–720, May 1998.
23. J. C. Tan, J. Silk, and C. Balland, “A Semiempirical Model of the Infrared Universe,” *ApJ* **522**, pp. 579–589, Sept. 1999.

24. T. T. Takeuchi, T. T. Ishii, H. Hirashita, K. Yoshikawa, H. Matsuhara, K. Kawara, and H. Okuda, "Exploring Galaxy Evolution from Infrared Number Counts and Cosmic Infrared Background," *PASJ* **53**, pp. 37–52, Feb. 2001.
25. L. Olmi, "Optical designs for submillimeter-wave spherical-primary (sub)orbital telescopes and novel optimization techniques," in *Highly Innovative Space Telescope Concepts Edited by Howard A. MacEwen. Proceedings of the SPIE, Volume 4849, pp. 245-256 2002.*, pp. 245–256, Dec. 2002.
26. J. Glenn, J. J. Bock, G. Chattopadhyay, S. F. Edgington, A. E. Lange, J. Zmuidzinas, P. D. Mauskopf, B. Rownd, L. Yuen, and P. A. Ade, "Bolocam: a millimeter-wave bolometric camera," in *Proc. SPIE Vol. 3357, p. 326-334, Advanced Technology MMW, Radio, and Terahertz Telescopes, Thomas G. Phillips; Ed.*, pp. 326–334, July 1998.
27. B. Rownd, J. J. Bock, G. Chattopadhyay, J. Glenn, and M. J. Griffin, "Design and performance of feedhorn-coupled bolometer arrays for SPIRE," in *Millimeter and Submillimeter Detectors for Astronomy. Edited by Phillips, Thomas G.; Zmuidzinas, Jonas. Proceedings of the SPIE, Volume 4855, pp. 510-519 (2003).*, pp. 510–519, Feb. 2003.
28. M. J. Griffin, J. J. Bock, and W. K. Gear, "Relative performance of filled and feedhorn coupled focal plane architectures," *Appl. Opt.* **41**, pp. 6543–6554, Nov. 2002.